Brain Stimulation 14 (2021) 588–597

Contents lists available at ScienceDirect

Brain Stimulation

journal homepage: http://www.journals.elsevier.com/brain-stimulation

Effects of direct current stimulation on synaptic plasticity in a single neuron

Forouzan Farahani [a, *], Greg Kronberg [a], Mohamad FallahRad [a], Hysell V. Oviedo [b, c], Lucas C. Parra [a]

[a] Department of Biomedical Engineering, The City College of New York, New York, NY, USA
[b] Biology Department, The City College of New York, New York, NY, USA
[c] CUNY Graduate Center, New York, NY, USA

ARTICLE INFO

Article history:
Received 13 October 2020
Received in revised form
2 February 2021
Accepted 3 March 2021
Available online 22 March 2021

Keywords:
Transcranial electric stimulation
Transcranial direct current stimulation
Synaptic, plasticity
Long-term potentiation
tDCS
LTP

ABSTRACT

Background: Transcranial direct current stimulation (DCS) has lasting effects that may be explained by a boost in synaptic long-term potentiation (LTP). We hypothesized that this boost is the result of a modulation of somatic spiking in the postsynaptic neuron, as opposed to indirect network effects. To test this directly we record somatic spiking in a postsynaptic neuron during LTP induction with concurrent DCS.

Methods: We performed rodent in-vitro patch-clamp recordings at the soma of individual CA1 pyramidal neurons. LTP was induced with theta-burst stimulation (TBS) applied concurrently with DCS. To test the causal role of somatic polarization, we manipulated polarization via current injections. We also used a computational multi-compartment neuron model that captures the effect of electric fields on membrane polarization and activity-dependent synaptic plasticity.

Results: TBS-induced LTP was enhanced when paired with anodal DCS as well as depolarizing current injections. In both cases, somatic spiking during the TBS was increased, suggesting that evoked somatic activity is the primary factor affecting LTP modulation. However, the boost of LTP with DCS was less than expected given the increase in spiking activity alone. In some cells, we also observed DCS-induced spiking, suggesting DCS also modulates LTP via induced network activity. The computational model reproduces these results and suggests that they are driven by both direct changes in postsynaptic spiking and indirect changes due to network activity.

Conclusion: DCS enhances synaptic plasticity by increasing postsynaptic somatic spiking, but we also find that an increase in network activity may boost but also limit this enhancement.

© 2021 The Author(s). Published by Elsevier Inc. This is an open access article under the CC BY-NC-ND license (http://creativecommons.org/licenses/by-nc-nd/4.0/).

Introduction

Transcranial direct current stimulation (tDCS) involves low-intensity electrical current applied to the brain via electrodes placed over the scalp [1]. tDCS has been used in a variety of human cognitive experiments [2] and clinical trials [3,4]. While there is a heated ongoing debate about the robustness of these effects in human trials [5], the evidence for the effects of direct current stimulation (DCS) on neural activity in animal studies is extensive [6,7]. We and others have noted that the stimulation intensity of tDCS in human experiments is typically less than 1 V/m [8], whereas in animal experiments it is often much larger [9]. For in vitro experiments, it is common to operate at 10 V/m or even 20 V/m and there are many reports of lasting effects under these conditions [10–12]. While this suggests that higher stimulation intensities may be required in human experiments, some have argued that stronger fields may lead to an inversion of the DCS effects [13,14].

Another open question is how the effects of DCS can outlast the period of stimulation. In human experiments, stimulation is usually applied for short periods of time, typically no more than 20 min, and effects are measured in the subsequent minutes, hours, or days. It is often argued that these lasting neural and cognitive effects are mediated by synaptic plasticity [15]. Specifically, some argue that tDCS can modulate endogenous synaptic plasticity [11,12,16,17],

* Corresponding author.
E-mail addresses: forouzan.v.farahani@gmail.com, fvasheg000@citymail.cuny.edu (F. Farahani).

https://doi.org/10.1016/j.brs.2021.03.001
1935-861X/© 2021 The Author(s). Published by Elsevier Inc. This is an open access article under the CC BY-NC-ND license (http://creativecommons.org/licenses/by-nc-nd/4.0/).

while others argue that tDCS has a lasting effect on neuronal excitability [10], or that it upregulates neurotrophic factors, such as BDNF that facilitates subsequent synaptic plasticity [16].

One mechanistic hypothesis is that DCS interacts with concurrent endogenous mechanisms of synaptic plasticity [11,12]. Specifically, DCS modulates postsynaptic activity which in turn affects synaptic plasticity as it is dependent on coincident pre- and postsynaptic activity. Therefore, by pairing plasticity inductions with concurrent DCS, one can observe lasting effects of DCS on synaptic efficacy [11,12]. This has been demonstrated in vitro for two classic induction plasticity protocols, namely, tetanic stimulation [11] and theta-burst stimulation [12]. Of particular, interest is theta-burst stimulation (TBS) because it is thought to more closely emulate endogenous plasticity mechanisms in the brain [18]. Furthermore, we have shown with TBS that the effects of DCS follow a number of properties of Hebbian plasticity, such as pathway-specificity and associativity [12]. These properties are important in the context of human learning because they are thought to underline the specificity of learning and our ability to associate related items [19–22]. A central claim of this hypothesis is that DCS boosts spiking on postsynaptic neurons during plasticity induction with TBS [12]. We hypothesized that this is the result of a modulation of somatic spiking with DCS in the postsynaptic neuron, as opposed to indirect network effects. While there is support for this claim from extracellular field recordings in vitro [12], there is no direct measurement of somatic spiking in postsynaptic neurons in the presence of DCS. It is possible that the LTP effects of DCS recorded extracellularly are mediated by indirect network effects. The goal of this work is to bridge this gap, and more specifically, to test whether explicitly controlling postsynaptic spiking can abolish or emulate the effects of DCS during plasticity induction with TBS.

There is extensive in vivo, in vitro, and in silico evidence that DCS can incrementally polarize the soma and therefore acutely modulate somatic spiking during DCS [23–25]. We know that "anodal" stimulation depolarizes the soma and can acutely increase firing rate [23,24]. It is well established that long-term potentiation of synapses induced with TBS is dominated by postsynaptic somatic firing [12]. Therefore anodal DCS should, and indeed does boost LTP induced by TBS [12]. Here, we aim to directly measure postsynaptic somatic firing in individual neurons using patch-clamp recordings and link this to the effects on LTP. To test our hypothesis, we recorded somatic spiking induced by TBS during DCS in the individual neuron. To isolate network effects and demonstrate a causal effect on the single neuron, we emulate anodal somatic depolarization with DCS by injecting depolarizing current, as well as suppress the effect of anodal DCS with an injected hyperpolarizing current. We record from pyramidal neurons in a classic hippocampal CA1 rodent preparation [26]. We also use a computational multi-compartment model of a pyramidal neuron to estimate the effects of the various interventions on membrane polarization, spiking activity, and synaptic plasticity. Overall, these single-cell experiments largely confirm our mechanistic hypothesis – with one caveat – namely, the effects of DCS on the whole network can not be ignored.

Results

Anodal DCS boosts LTP and somatic spiking

It is well established that during DCS neuronal compartments near the cathode are depolarized and compartments near the anode are hyperpolarized [27]. Given the orientation of pyramidal neurons – with the somatic compartment further away from the cortical surface – "anodal" stimulation depolarizes their somas [27].

In order to test the effects of this polarization on somatic firing and synaptic plasticity in single neurons, we performed whole-cell patch-clamp recording from pyramidal neurons in hippocampal CA1 (Fig. 1A). We used a TBS pulse-train (Fig. 1B) that is known to cause robust LTP in hippocampal slices [26]. Plasticity was induced in synapses relatively close to the soma (100 μm) targeting proximal apical dendrite. Action potentials propagate reliably from the soma to synapses at this distance. Synaptic potentiation was measured based on changes in the peak amplitude of the excitatory postsynaptic potential in response to a single-pulse probe (normalized EPSP, see Fig. 1C and Methods). Following earlier studies, GABAergic inputs were blocked to prevent the effect of direct activation of inhibitory interneurons [28]. The input resistance didn't change significantly before and after induction (Fig. 1E; control: $t(50) = -0.97$, $p = 0.33$; anodal: $t(50) = -0.89$, $p = 0.37$, here and in all subsequent pairwise comparisons we used a *t*-test) attesting to the stability of the recording setup. Pairing DCS with TBS led to an increase in synaptic potentiation (Fig. 1D, control:1.18 ± 0.42, N = 26 cells; anodal: 1.46 ± 0.42, N = 26 cells, $t(50) = 2.38$, $p = 0.0207$). Normalized EPSP is EPSP divided by baseline EPSP. To rule out changes in baseline EPSP as a potential confound, we confirmed that they did not differ between stimulation conditions (Fig. 1F; two-sample *t*-test: $t(50) = 0.95$, $p = 0.34$). We also measured the number of spikes during LTP induction with the TBS. Consistent with our hypothesis, the number of somatic spikes during TBS increased with anodal polarization (Fig. 1G, control: 7.84 ± 10.26; anodal: 27.53 ± 9.49, $t(50) = 7.166$, $p = 3.28 \times 10^{-9}$). Importantly, synaptic potentiation appears to be positively correlated with somatic spiking (Fig. 1H, Pearson's correlation $r = 0.38$). This was confirmed with a linear mixed effect model for normalized EPSP with spike count as linear covariate and stimulation condition as categorical covariate on the offset. We found a significant effect of stimulation condition ($t(50) = 12.1$, $p = 1.8 \times 10^{-16}$) and of spike count ($t(50) = 2.9$, $p = 0.005$). Given that the stimulation affects spike count, we conclude that increased spiking is a viable explanation for the effects of DCS on LTP.

Effects of DCS can not be fully emulated or abolished with somatic current injection

To demonstrate a causal link between enhanced spiking induced by DCS and enhanced LTP, we implemented two additional conditions (Fig. 2A and B). First, to emulate the effects of anodal DCS on somatic depolarization and spiking, we injected a positive current into the soma in the absence of DCS. Earlier in vitro studies in both hippocampal and cortical slices demonstrated that the soma of pyramidal neurons is polarized on average by 0.15 V per V/m of electric field, so that 20 V/m are expected to polarize the soma by 3 mV [29,30]. The amount of depolarization due to DCS is also validated with a biophysically-realistic, and empirically-validated computational model of a CA1 pyramidal neuron (Fig. 2C). This somatic depolarizing current injection increased the number of somatic spikes (Fig. 2H, $t(71) = -3.30$, $p = 0.0014$) and enhanced LTP over the control condition (Fig. 2D & E; control: 1.19 ± 0.43, N = 48 cells; depolarizing current injection: 1.86 ± 0.81, N = 25 cells, $t(71) = -4.62$, $p = 1.63 \times 10^{-5}$).

In a second condition, we applied DCS but injected a hyperpolarizing current to oppose the resulting somatic depolarizing (Fig. 2A and B). As predicted, this hyperpolarizing current reduced the number of somatic spikes compared to anodal DCS alone (Fig. 2H, $t(48) = 3.25$, $p = 0.002$). The current injection here was calibrated to shift the somatic membrane polarization by 3 mV. However, this may not have been sufficient to compensate for the effect of anodal DCS as the number of spikes was still significantly higher than in the control condition (Fig. 2D & H, control: 8 ± 10.44;

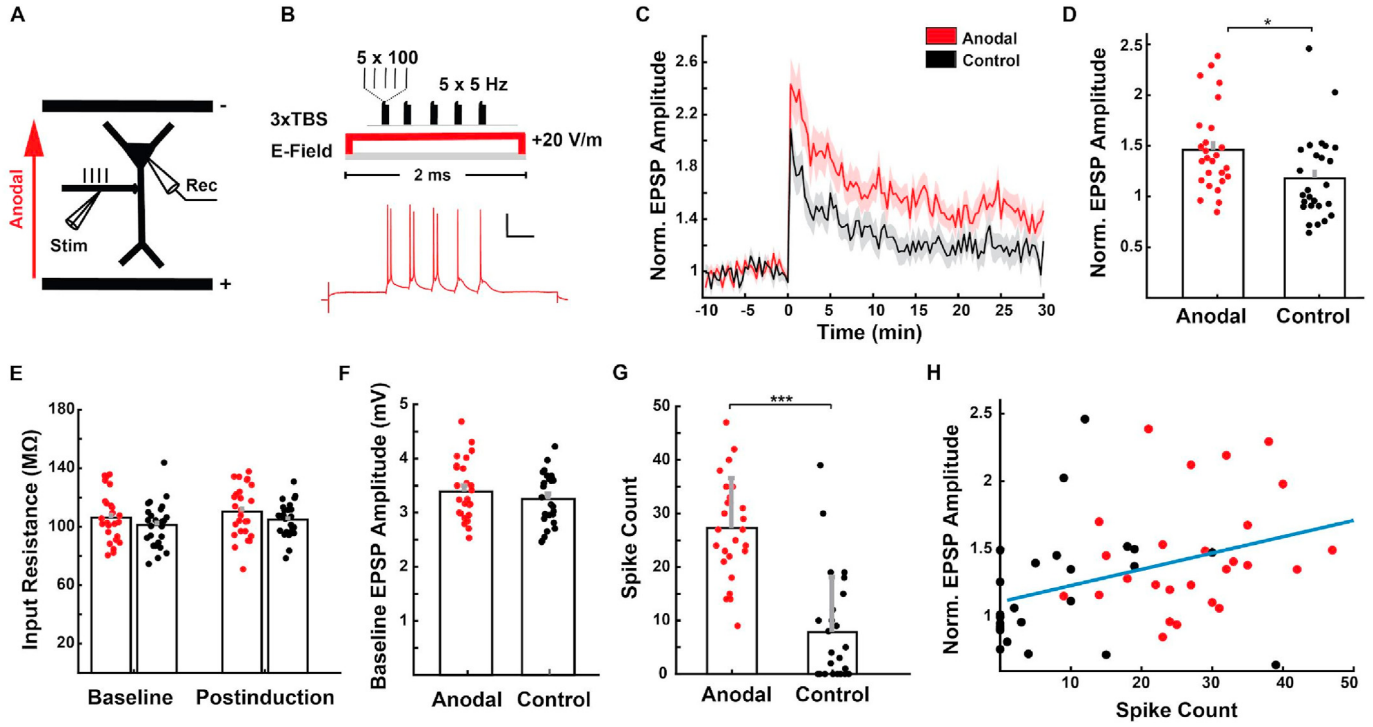

Fig. 1. **A:** Experimental configuration with whole-cell somatic patch-clamp recording and stimulation of Schaffer-Collateral fibers in the presence of an electric field (red) caused by anodal DCS. **B:** Top: TBS pulse pattern. TBS: Bursts of 5 pulses at 100 Hz were repeated 5 times at 5 Hz (1s total). This 1s TBS was repeated three times with 30 s spacing. Bottom: a sample trace of voltage recorded during TBS with DCS. The scale bars represent 20 mV and 200 ms **C:** Traces of averaged normalized EPSPs amplitude for anodal condition (red, DCS) and control condition (black, no DCS). LTP was induced at time = 0. **D:** Normalized EPSP amplitude. **E:** Input resistance before and after induction. **F:** Baseline EPSP amplitude in different stimulation conditions. **G:** Number of spikes during theta burst stimulation. **H.**Normalized EPSP amplitude vs. spike count. The blue line represents the linear regression between the spike count and normalized EPSP amplitude. Significant differences indicated as * $p < 0.05$, ** $p < 0.01$, *** $p < 0.001$, n.s. $p > 0.05$. (For interpretation of the references to colour in this figure legend, the reader is referred to the Web version of this article.)

anodal with hyperpolarizing current injection: 16.91 ± 13.31; two-sample *t*-test $p = 1.7 \times 10^{-4}$). Indeed, the boost of LTP with DCS, was not abolished by this hyperpolarizing current (control: 1.19 ± 0.43, N = 48; anodal with hyperpolarizing current injection: 1.46 ± 0.74, N = 24 cells, p = 0.06). To rule out methodological confounds, we again checked for membrane resistance and found that it was unaltered for the two new conditions (Fig. 2F). In addition, we did not find a significant difference in baseline EPSPs across different stimulation conditions to prevent the possible confound (Fig. 2G, one-way ANOVA: $F(3) = 0.61$, $p = 0.61$).

So far the results are consistent with our somatic spiking hypothesis. Indeed, there is a clear correlation between somatic spiking and LTP across all conditions (Fig. 2I, $r = 0.42$). To rule out that this effect is driven by the stimulation condition alone, we used again a linear mixed effect model and find an effect of spike count ($t(121) = 5.2$, $p = 8.9 \times 10^{-7}$) and stimulation condition ($t(121) = 15.2$, $p = 5.4 \times 10^{-30}$). Indeed, when analysing the control condition alone (for which we have sufficient statistical power) we found a significant correlation between spike count and LTP ($r(46) = 0.31$, $p = 0.03$) replicating a well-established finding [31,32]. However, contrary to our expectations, despite a significant increase in the number of spikes between anodal DCS and depolarizing current injection ($t(49) = 2.99$), $p = 0.0043$) we did see a decrease in LTP relative to depolarizing current injection ($t(49) = -2.25$, $p = 0.0289$). Given the larger number of spikes, we would have expected a larger effect of anodal DCS on LTP. We note, however, that there is a fundamental difference between DCS and current injection, namely, depolarizing current injection affects only a single neuron, whereas DCS affects all neurons in the network.

DCS-induced network spiking in neurons

A clue that other neurons in the network can not be ignored during anodal DCS comes from the observation of induced network spiking before the onset of TBS (Fig. 3A). We will refer to these action potentials as early spikes. We observed early spikes in 8 of 26 neurons during anodal DCS with 20 V/m (Fig. 3D). When the DCS magnitude is reduced to 10 V/m these early spikes are absent (Fig. 3C), which is a significant drop (Fisher exact: $p = 0.018$, with FDR correction: $P = 0.027$). Injecting a hyperpolarizing current also reduced the number of cells exhibiting early spikes (Fisher exact test $p = 0.076$, FDR correction: $p = 0.076$). In order to observe LTP in the experiments above it was necessary to block inhibitory input (with GABA-A and GABA-B antagonists), consistent with previous literature [26,28,33]. When inhibitory inputs were left intact early spikes also disappeared (Figs. 3B and 0 of 20 neurons), which is again a significant drop (Fisher Exact test: $p = 0.0064$, with FDR correction: $p = 0.0192$). Given the dependence of these early spikes on electric field magnitude and GABAergic input, we conjecture that strong fields induced network firing which is amplified by recurrent excitatory connections within the CA1 network.

Computational modeling explains results as single neuron effects and unspecific effect on network activity

To reconcile and explain these results we implemented a biologically realistic model of a CA1 pyramidal neuron (Fig. 4A). This 3D anatomically realistic multi-compartment model of CA1 rat pyramidal cell includes experimentally-validated membrane voltage dynamics [30]. The effects of DCS on membrane voltage are

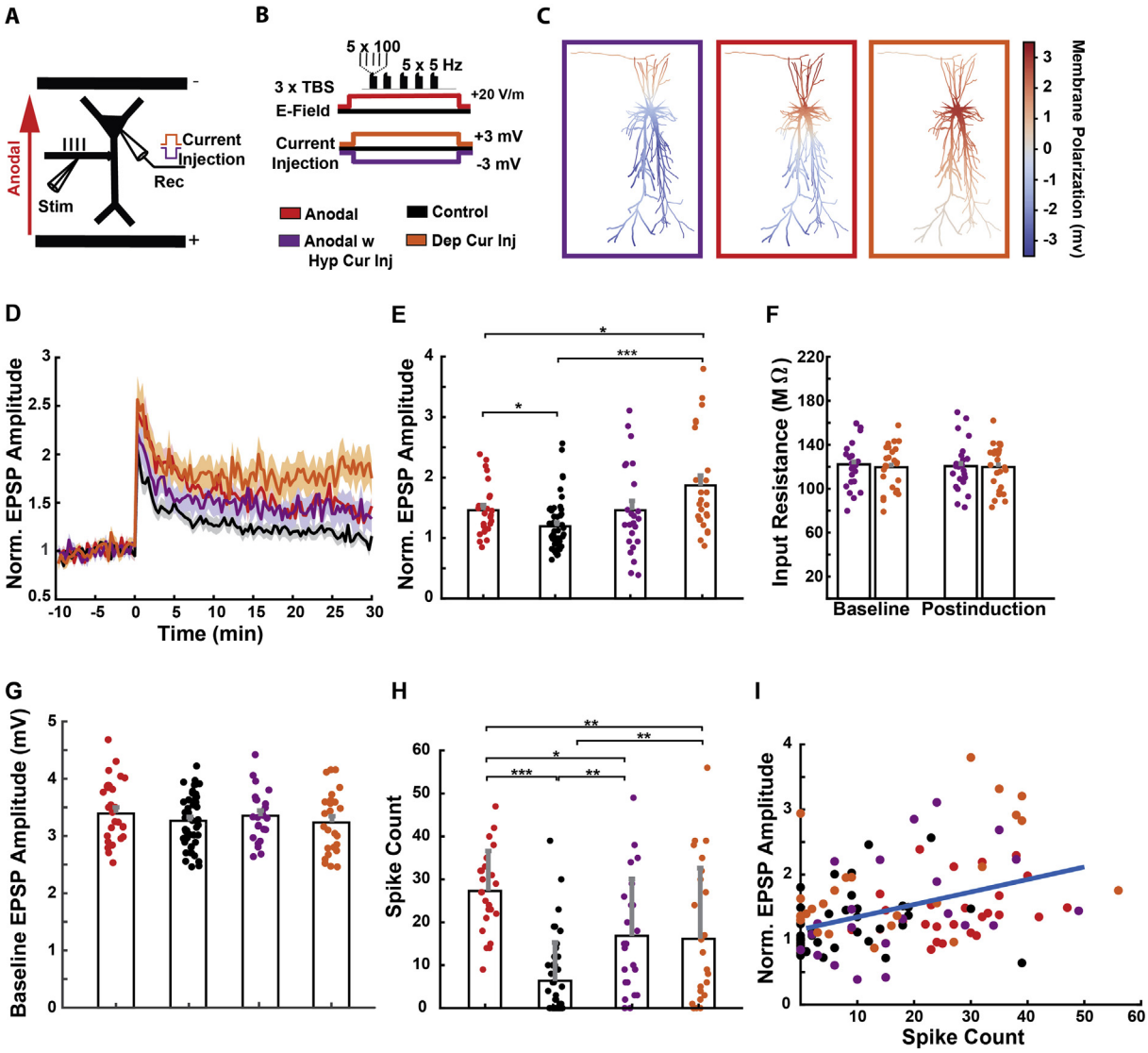

Fig. 2. **A:** Experimental setup. **B:** Illustration of induction protocol. **C:** Membrane polarization with somatic current injection in a multicompartment neuronal model. Left: Somatic hyperpolarizing current injection with anodal DCS, Middle: anodal DCS, Right: Somatic depolarizing current injection. **D:** Traces of average normalized EPSP amplitude. **E:** Normalized EPSP amplitude in different conditions: anodal (N = 26 cells), control (N = 48 cells), anodal with hyperpolarizing somatic current injection (N = 24 cells), and depolarizing somatic current injection (N = 25 cells). **F:** Input resistance before and after LTP induction **G:** Baseline EPSP amplitudes in different stimulation conditions. **H:** The number of spikes after the first pulse of the first burst and 25 ms after the last pulse in the last burst. **I:** Positive correlation of LTP with somatic spiking across all cells and experimental conditions. The blue line represents the linear regression between the spike count and normalized EPSP amplitude. (For interpretation of the references to colour in this figure legend, the reader is referred to the Web version of this article.)

implemented by applying an extracellular voltage gradient as described previously [12]. Also following this work we implement a standard voltage-dependent plasticity rule, which reproduces extensive experimental results on LTP [34]. While this single-neuron model (M1) shows an increase in spiking and LTP for anodal stimulation over control it does not replicate the observed excess of spiking above the condition with a depolarizing current injection (Fig. 4B, M1). Please see Methods for details on the model neuron, implementation of DCS effects and the plasticity rule.

We postulate that this excess spiking is the result of elevated network activity induced by DCS which impinges on the single test neuron. To emulate this effect of DCS in the model we added synapses located at the basal and apical dendrites and activated them at random with independent Poisson spike trains. This model (M2) replicates the experimental results of the firing rate for all conditions (Fig. 4B, M2). However, this increase in spiking further enhances LTP for DCS in disagreement with experiments, in particular when spiking was limited by hyperpolarizing current (Fig. 4C, M2). In model M2, this effect is the result of dendritic membrane polarization, and occurs even if somatic spiking is reduced by somatic injection of hyperpolarizing current (Fig. 4D). To reconcile the model with experiment, we considered the effect of this enhanced network activity on LTP. There is prior evidence for a homeostatic mechanism, whereby elevated network activity can suppress LTP due to the depletion of extracellular calcium, which is affected by neighboring synapses including from nearby neurons [35]. Following this work, we include a term to the plasticity rule, which depends on extracellular calcium that is depleted in the presence of elevated network firing. With this model (M3) of the effects of network activity, we now replicate the experimental results on spiking and LTP (Fig. 4C, M3). In total, the model M3 best

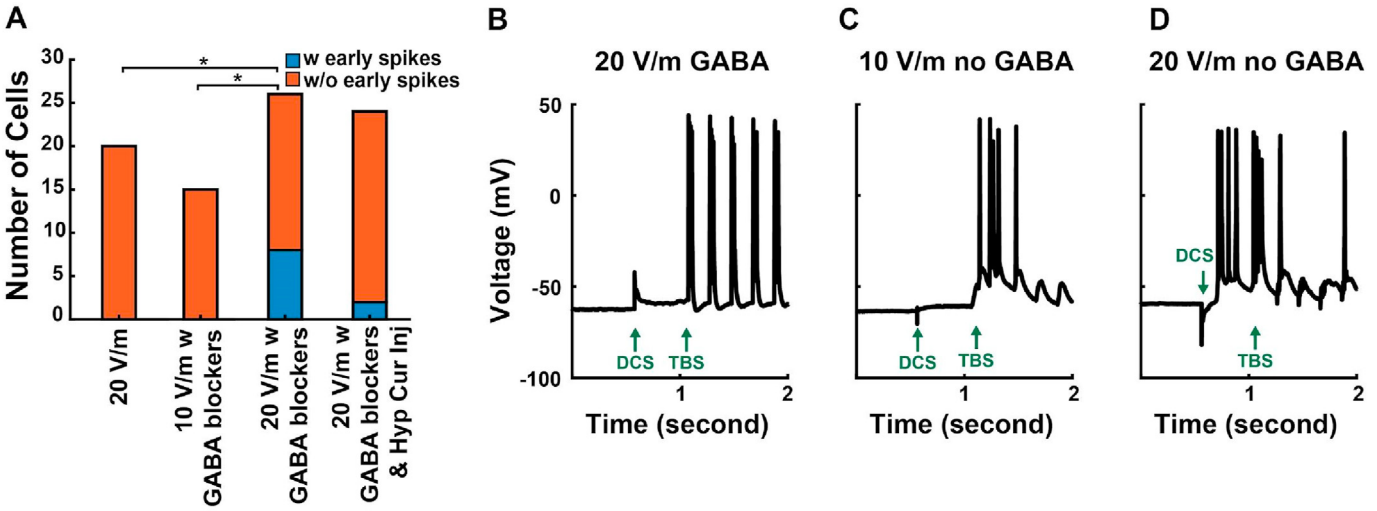

Fig. 3. Example traces of whole-cell recording during induction. **A:** Number of cells exhibiting action potentials before TBS onset. Fisher exact test with FDR. *p < 0.05 (20 V/m vs. 20 V/m with GABA blocker) and *p < 0.05 (10 V/m with GABA blocker vs. 20 V/m with GABA blocker). **B:** firing was evoked by a stimulator while GABAergic inputs were intact under 20 V/m electric field (N = 20 cells). The gray area shows the period prior to TBS and after DCS onset. **C:** firing was evoked by a stimulator under 10 V/m when GABA antagonists were added. **D:**neuronal firing was evoked by a stimulator electrode under 20 V/m electrode when GABA antagonists were added.

replicates the pattern of spiking (Fig. 4B) and LTP observed across the 4 experimental conditions (Fig. 4C).

These modeling results suggest that we should distinguish between spikes evoked during TBS versus early spikes that likely reflect induced network activity by DCS. According to the model,

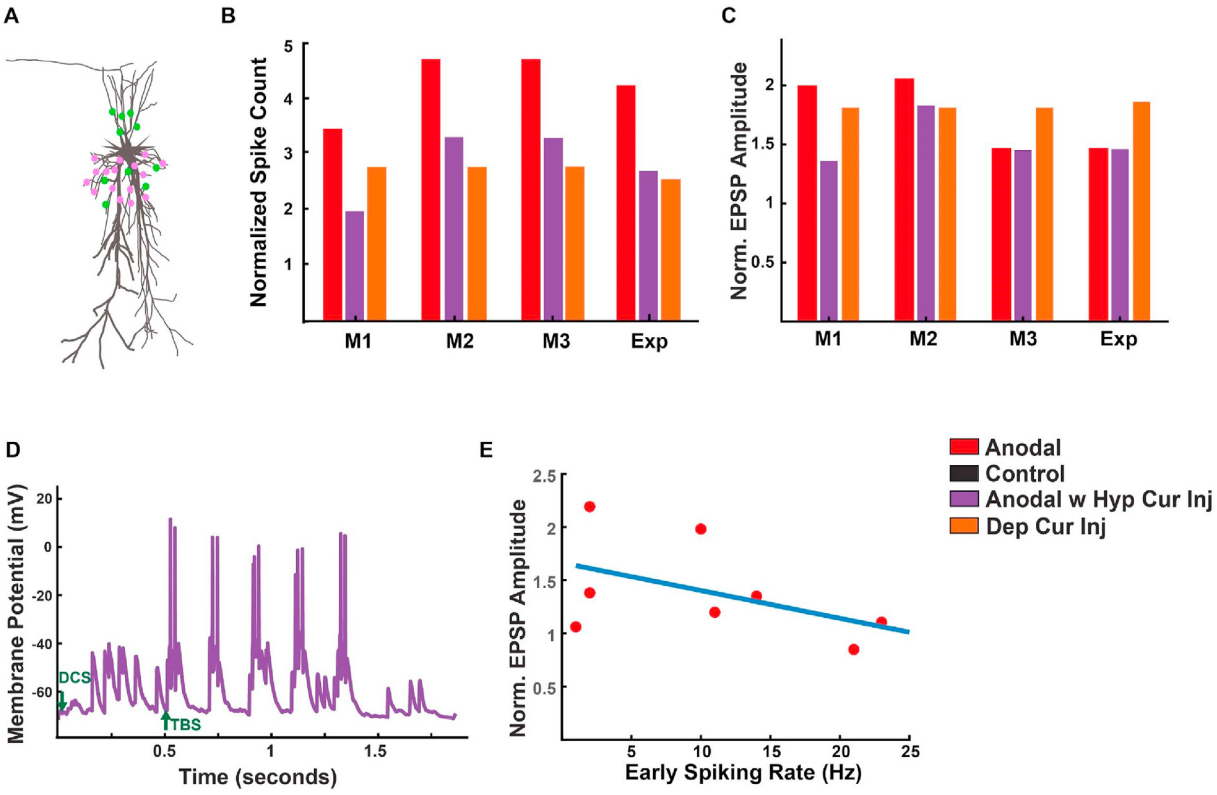

Fig. 4. Computational modeling. **A:** Simulated biophysically realistic CA1 pyramidal neuron with synapses stimulated by applied TBS (pink) and synapses stimulated by induced network activity due to DCS (green). **B:** Spike count is normalized here relative to the control condition to compensate for differing overall spiking (3.3 vs 2.6 spikes per TBS for model vs experiment, respectively). Models include single-neuron model (M1), model including DCS-induced network activity (M2), model including homeostatic plasticity (M3) and experiment (Exp) **C:** For experiments this shows the normalized EPSP amplitude. For models this shows the normalized synaptic efficacy relative to control condition (see Methods). **D:** Sample of dendritic membrane potential in Anodal DCS with hyperpolarizing current injection shows depolarization due to induced network activity, e.g. before TBS. **E:** Normalized EPSP amplitude vs. early spiking rate. The blue line represents the linear regression between the early spiking rate and normalized EPSP amplitude. (For interpretation of the references to colour in this figure legend, the reader is referred to the Web version of this article.)

the number of evoked spikes should be positively correlated with LTP, which was born out by the experiment (Fig. 1H). While we find a negative correlation with the number of early spikes where they occur (N = 8), it does not reach significance ($r(6) = -0.48$, $p = 0.22$).

Discussion

The goal of most tDCS experiments in humans is to induce specific changes in behavior that outlast the period of stimulation. Synaptic plasticity is a putative mechanism to mediate such specific and lasting effects [11,12,14,16,36]. Our previous in vitro experiments suggested that DCS can enhance ongoing Hebbian synaptic plasticity by modulating the membrane potential of neurons [11,12]. Extracellular recordings during DCS provided indirect evidence that synaptic plasticity is modulated by DCS effects on dendritic membrane polarization [11] as well as effects on somatic spiking [12]. The present whole-cell recordings show an effect of DCS on postsynaptic spiking, which in turn modulates synaptic plasticity of individual neurons, suggesting a highly specific effect of DCS. However, we also see evidence that DCS, at high field magnitudes, induced spontaneous network activity, which may lack the specificity of Hebbian plasticity. This induced network activity boosts but also limits the effect on LTP through a homeostatic mechanism.

To show that acute membrane depolarization is directly implicated in the effects of DCS, we injected current to emulate or abolish the somatic membrane polarization expected as a result of DCS. The results are consistent with the hypothesized causal role of membrane somatic depolarization. However, the injected somatic current may not have entirely emulated/abolished the effect of DCS on membrane polarization, as it was calibrated to an average sensitivity reported by earlier studies [27,29,30], rather than the sensitivity of the individual neuron. Therefore, the mismatch in observed LTP with the simpler model of our hypothesis may be partially explained by a miscalibration. But also, we were forced to introduce an effect of DCS on spontaneous network activity in order to reconcile the computational model with the experimental data.

Evidence that network activity could affect synaptic efficacy through a homeostatic mechanism comes from a study on spike-timing-dependent plasticity (STDP) [35]. This study suggests that bursting network activity may deplete extracellular calcium concentration and thus limit LTP. Such homeostatic regulation may serve to counteract run-away potentiation. Motivated by a computational model of this effect, we searched for a correlation with DCS-induced spiking but the negative correlation with LTP was not significant. This homeostatic mechanism reconciled the empirical observation that the boost of LTP was limited despite a substantial increase in postsynaptic spiking during strong anodal DCS (20 V/m).

We inferred that the induced spiking activity observed here during DCS may result from the activation of recurrent connections between CA1 pyramidal neurons. Although we do not provide direct evidence for this, there are several factors supporting this interpretation. First, the DCS-induced activity required the removal of GABAergic inhibition, which normally limits the spread of activity via recurrent excitatory connections. Second, our slice preparation removes the CA3 area so that we can rule out DCS activation of CA3 pyramidal neurons. Finally, these CA1 recurrent connections synapse to the basal and apical dendrites [37–39] and the experiment and model match one another when we replicate this feature.

Earlier studies demonstrated that electric fields <30 V/m were not strong enough to induce activity in cortical [29] and hippocampal slices [30]. However, our results suggest that spontaneous activity can be evoked by electric fields with an intensity of 20 V/m in the presence of GABAergic input blockers. While blocking GABA receptors is common in hippocampal LTP studies [26,28,33], this manipulation is merely intended to facilitate the study of excitatory plasticity and does not model normal physiology. Similarly, we use 20 V/m fields here to more reliably detect small effects with limited sample sizes, as is common in the literature [11,12]. A caveat of our study is that cortical electric fields during typical human tDCS experiments are known to be < 1 V/m, a full order of magnitude lower [8]. An important question is therefore whether these effects persist under physiological levels of inhibition and lower electric field magnitudes. Another caveat is that tDCS mostly reaches cortical regions, while the present study analyzed hippocampal pyramidal cells often used in LTP studies due to the well-segregated input pathways. However, the basic mechanisms identified here should generalize to cortical effects of DCS.

In principle, direct effects of tDCS on the firing of individual cells can be propagated throughout any network via recurrent excitatory connections, suggesting that similar but weak effects may persist under physiological conditions [40]. The propagation of excitatory activity in a network is particularly sensitive to the balance of excitatory and inhibitory synaptic connection strengths [41–43], suggesting that these effects need to be directly tested under more physiological conditions. Indeed, more physiologically realistic preparations show that weak DCS can have acute modulatory effects on endogenous gamma activity [24]. The same preparation also shows lasting plasticity of DCS that are purely enhancing [44]. What we show here is that network activity may have also constrained this enhancing effect. Known homeostatic plasticity mechanisms depend on neuronal firing [45], and conceivably the effects of tDCS on neuronal excitability can in principle recruit these mechanisms [46]. Regardless, network effects are likely to be less specific than the pathway specific mechanisms studied with classic plasticity induction mechanisms [12] We conclude that the specific effects of DCS will depend strongly on the endogenous network activity, which motivates future research with more realistic preparations.

As with our previous studies [11,12,47], the effects of DCS during plasticity induction have again been to increase synaptic efficacy. Here we activated synapses at the proximal apical dendrites as they are expected to be dominated by somatic polarization. Therefore anodal DCS is depolarizing and thus boosts LTP. For distal apical dendrites, DCS causes the opposite polarization and therefore a boost of LTP required cathodal DCS [11].

In conclusion, we provide the first direct evidence linking the effects of DCS on neuronal membrane potential and excitability to Hebbian synaptic plasticity. While this mechanism now has some support [12,48,49], we also uncovered that it cannot fully account for the effects of DCS on plasticity. We propose that DCS also affects plasticity via the propagation of DCS effects over recurrent excitatory connections in combination with a homeostatic plasticity mechanism. These mechanisms may also help account for several features of human tDCS experiments which are difficult to explain with a Hebbian mechanism alone, such as effects of tDCS when applied prior to training [50] or previous reports of highly nonlinear dose-response functions in humans [13,14]. The degree to which these mechanisms contribute to the effects of tDCS in humans is an exciting area for future research.

Methods

Slice preparation

All animal procedures were approved by the Institutional Animal Care and Use Committee At The City College of New York, CUNY (protocol 2016–24). 3-5-week-old male Wistar rats were anesthetized by Ketamine and Xylazine injection and were euthanized

by cardiac perfusion with an artificial cerebrospinal fluid (ACSF) containing (in mM): 110 choline chloride, 3.2 KCl, 1.25 NaH2-PO4,26NaHCO3, 0.5 CaCl2,7 MgCl2, 2 ascorbate, 3 pyruvate and 10 D-glucose. After cardiac perfusion, the whole brain was transferred to an ice-cold dissection chamber containing the same ACSF solution. The dissection chamber was mounted on a vibrating microtome (Campden Instruments) and transverse hippocampal brain slices were obtained with 400-μm thickness. The CA3 area was cut to limit recurrent excitatory connections and prevent seizure-like activity in experiments that involved GABA blockers. After dissection, slices were transferred to a recovery chamber at 34 °C for 30 min with a modified ACSF solution containing (in mM): 124 NaCl, 3.2 KCl, 1.25 NaH2PO4, 26 NaHCO3, 2.5 CaCl2, 1.3 MgCl2, 2 ascorbate, 3 pyruvate, and 25 D-glucose. After 30 min of recovery, slices were then transferred to a holding chamber at 30 °C for at least another 30 min with the recording ACSF containing (in mM): 124 NaCl, 3.2 KCl, 1.25 NaH2PO4, 26NaHCO3, 2.5 CaCl2, 1.3 MgCl2, 25 D-glucose. After at least 30 min in the holding chamber slices were transferred to a recording chamber perfused with the same recording ACSF for experiments. All ACSF solutions were saturated with a carbogen gas mixture containing 95% O2 and 5% CO2.

Whole-cell electrophysiology recording in vitro

Slices were perfused in a submerged chamber (Harvard Apparatus) with oxygenated recording ACSF with a flow rate of 1–1.5 ml/min. The temperature of the chamber was set to 30 °C using both inline and chamber temperature controllers. For most experiments, GABA-A and GABA-B inputs were blocked by adding 2 μM of SR 95531 and 1 μM of CGP52432 to the recording ACSF, respectively. In the presence of GABA antagonists in the ACSF, the intracellular solution contained (in mM): 115 K-Gluconate, 20 KCl, 10 Na2-phosphocreatine, 10 HEPES, 4 Mg-ATP, 0.3 Na-GTP followings [26]. Otherwise, the intracellular solution contained (in mM): 128 K-Gluconate, 10 Na2-phosphocreatine, 10 HEPES, 4 Na-ATP, 0.4 Na-GTP, 4 MgCl2 following [51]. Raw electrical signals were amplified with a MultiClamp 700B amplifier and then low-pass filtered at 10 kHz and sampled at 20 KHz with a 1550B Digitizer (Molecular Devices). The resistance of patch pipettes was within 3–5 MΩ. Patch pipette series resistance was always lower than 40 MΩ.

After anchoring the slice in the chamber, two parallel Ag–AgCl wires with 1 mm diameter were placed on opposite sides of the slice with the slice equidistant from each wire. DCS was applied as a constant current between the wires (Caputron LCI 1107 High Precision). The slice and field wires were oriented so that the applied electric field was parallel to the somatodendritic axis of CA1 pyramidal neurons. Anodal stimulation was applied such that CA1 apical dendrites were closer to the positive electrode and CA1 basal dendrites were closer to the negative electrode. This configuration mimics the relative orientation of cortical pyramidal cells when current flows inward from the cortical surface and depolarizes pyramidal neuron somas [27,29], which is assumed during anodal stimulation in humans. The applied current was calibrated to produce a 20 V/m electric field as measured by two electrodes placed in the slice.

To activate excitatory synapses, bipolar stimulation was applied using a theta glass electrode filled with ACSF (pulled by a Sutter Instruments P-97). The tip was then broken to produce a tip size of 15–20 μm. The stimulation electrode was placed in the apical dendrites, 100–150 μm away from the patched neuron toward CA2. Single excitatory postsynaptic potentials (EPSP) were evoked with probing stimuli of 5–100 μA amplitude and 60 μs duration square pulses. Probing stimulation amplitude was set to evoke an EPSP amplitude between 2 and 5 mV. EPSP amplitudes were measured as the peak amplitude of the difference between the membrane potential after a probe stimulus and the median of the membrane potential over 1 s time window before the probe stimulus. Once the probing stimulation amplitude was determined, baseline EPSPs were recorded every 20 s for at least 10 min. During baseline recording, input resistance was monitored by injecting −25 pA through the patch electrode 1 s after each probing stimulus. We divided the recorded voltage by the amount of current we injected to calculate input resistance. If the EPSP amplitude and membrane resistance were stable over the 10 min baseline period, TBS was applied to induce plasticity. TBS consisted of bursts of 5 pulses at 100 Hz, with each burst repeated 5 times at 5 Hz to compose an epoch, and each epoch repeated 3 times at 0.033 Hz (30 s inter-epoch interval). After TBS, baseline EPSPs were again recorded every 20 s for 30 min. For some experiments (Fig. 3), a monopolar stimulating electrode was used, instead of bipolar stimulating electrode, by pulling a regular glass capillary instead of theta glass. The other pole was then placed in the bath far away from the slice. For these monopolar experiments the TBS protocol was also changed to a single epoch consisting of 15 bursts at 5 Hz, with each burst again consisting of 5 pulses at 100 Hz.

For anodal DCS conditions, DCS started 500 ms before TBS and ended 500 ms after TBS. For conditions involving additional current injection with the patch electrode, this current injection was calibrated to produce a ±3 mV change in membrane potential at the soma. This calibration was done after establishing a stable baseline but before induction. Current injection through the patch electrodes was timed identically to the DCS condition, starting 500 ms before TBS and ended 500 ms after.

Data analysis

Normalized EPSP

To assess synaptic plasticity within a given slice, the average EPSP amplitude over the last 10 min (21–30 min after TBS) was calculated and normalized to the average of baseline EPSPs (normalized EPSP).

Spike count

Spikes were detected by thresholding membrane potential at −8 mV which is far from spike initiation threshold (~-50 mV). Then, spikes were counted over the period of TBS, starting with the first pulse and ending 25 ms after the last pulse. All the analyses were performed using MATLAB.

Computational Modeling

Multicompartmental simulations of a CA1 pyramidal neuron were performed using NEURON v7.7 [52] and Python v3.7. The detailed morphology of a CA1 pyramidal cell from an adult rat was obtained from a previous publication by Berzhanskaya et al. [30] (c62564 from NeuroMorpho.Org). The passive membrane properties were also set to have the same values as that work. We incorporated the active membrane properties similar as in Kronberg et al. [12] such as voltage gated channels and receptors. We only made a few adjustments as described below (Table 1).

The effects of DCS on the model neuron were implemented in NEURON by specifying an external potential gradient following [12]. Note that the model uses a single representative 3D neuron morphology, whereas in the experiment each recording was from different neurons, with potentially different morphology. Although we know that length and orientation of the neuron affects their sensitivity to DCS, we do not believe that the main findings of the computational work depend on these factors (other than in overall scale). Indeed, in the experiment we injected somatic currents assuming a single average sensitivity to DCS.

Table 1
Parameters for the neuron model.

Parameter	Value	Explanation
$g_{Na^+}^{dend}$	42- dg_{Na}*d mS*cm^{-2}	Voltage gated sodium conductance in dendrites decreases with distance d (in μm) from the soma
$g_{Na^+}^{soma}$	42 mS*cm^{-2}	Voltage gated sodium conductance in soma
$g_{Na^+}^{axon}$	105 mS*cm^{-2}	Voltage gated sodium conductance in axon
dg_{Na^+}	−0.2 mS*cm^{-2}	Gradient of voltage gated sodium conductance
E_{Na^+}	50 mV	Sodium reversal potential
$Sha_{V_{1/2}^{Na^+axon}}$	−4 mV	Parameter to shift the midpoint of activation curve of voltage gated sodium conductance in axon.
E_{K^+}	−77 mV	Potassium reversal potential
E_h	−30 mV	H-current reversal potential
$g_{K_{DR}^+}$	10 mS*cm^{-2}	Delayed rectifier potassium peak conductance
$g_{K_A^+}$	30 mS*cm^{-2}	A-type potassium peak conductance
g_h	.025*(1+2d/100) mS*cm^{-2}	H-channel conductance. Linearly increasing with distance d (in μm) from the soma
$V_{1/2}^{h_{prox}}$	−81 mV	Activation threshold for proximal (<100 μm from soma) h channel conductance
$V_{1/2}^{h_{dist}}$	−90 mV	Activation threshold for distal (>100 μm from soma) h channel conductance
τ_{ampa}^{close}	2 ms	AMPA receptor conductance decay time constant
τ_{ampa}^{open}	0.2 ms	AMPA receptor conductance rise time constant
τ_{nmda}^{open}	1 ms	NMDA receptor conductance rise time constant
τ_{nmda}^{close}	50 ms	NMDA receptor conductance decay time constant
g_{ampa}	1 nS	Peak AMPA receptor conductance
g_{nmda}	1 nS	Peak NMDA receptor conductance
τ_F	60 ms	Facilitation time constant
τ_{D_1}	540 ms	1st depression time constant
τ_{D_2}	45 ms	2nd depression time constant
τ_{D_3}	120 s	3rd depression time constant
f	2.8	Additive facilitation factor
d_1	0.68	1st Multiplicative depression factor
d_2	0.12	2nd Multiplicative depression factor
d_3	0.95	3rd Multiplicative depression factor
T	30 C	Temperature

For the axonal firing, the voltage sensitivity for activation of sodium channels was more hyperpolarized in the initial segment of axon compared with soma and dendrites as has been suggested in previous publications [53]. A gradient was considered for the density of sodium channels according to the findings of Kim et al. [26]. Every synapse was considered to have both AMPA and NMDA receptors. These receptors were modeled by the difference of two exponential functions as previously published by [Ref]. 16 synapses were selected randomly across the apical dendrites within 300 μm from the soma. This number of synapses was activated to mimic spiking activity due to TBS. We refer to this model as model 1 (M1).

In addition to modeling evoked synaptic input, we also modeled synaptic input due to the DCS induced network activity of other neurons in the CA1 network and we called it model 2 (M2). This network input was modeled as 10 synapses randomly distributed on the apical and basal dendrites, which activated via a poisson process. The number, weight and mean input rate of these synapses were manually fit to reproduce two aspects of the experimental spike data, the fraction of neurons exhibiting early spikes (after DCS onset, but before TBS onset) and the ratio of the total number spikes in each condition compared to control.

Normalized spike counts

We normalized the average of spike counts relative to the average of spike counts in the control condition.

Voltage-dependent synaptic plasticity rule

We adopted a voltage-dependent synaptic plasticity rule introduced by Clopath et al. in line with our previous work [12,34]. According to this plasticity rule, the arrival time of presynaptic input and postsynaptic membrane potential determines the amount of synaptic weight change as:

$$\frac{d}{dt}w_i = -A_{LTD}X_i(t)\left[\underline{u_-}(t)-\theta_-\right]_+ + A_{LTP}\underline{x_i}(t)[u(t)-\theta_+]_+\left[\underline{u_+}(t)-\theta_-\right]_+$$

where w_i represents to the weight of the i^{th} synapse, A_{LTD} and A_{LTP} correspond to parameters controlling LTD and LTP rate respectively, $X_i(t)$ is the presynaptic spike count, $\underline{x_i}(t)$ is the results of low-pass filtering $X_i(t)$, $\underline{u_-}(t)$ and $\underline{u_+}(t)$ are low-pass filtered of the post-synaptic potential $u(t)$ with different time constants, θ_- and θ_+ are LTD and LTP threshold parameters, and $[]_+$ is a heaviside function. The dynamics of $\underline{u_-}(t)$, $\underline{u_+}(t)$ and $\underline{x_i}(t)$ are considered as:

$$\tau_-\frac{d}{dt}\underline{u_-}(t) = -\underline{u_-}(t) + u(t)$$

$$\tau_+\frac{d}{dt}\underline{u_+}(t) = -\underline{u_+}(t) + u(t)$$

$$\tau_x\frac{d}{dt}\underline{x_i}(t) = -\underline{x_i}(t) + X_i(t)$$

The parameters used in the synaptic plasticity rule are summarized in Table 2. We quantified the overall synaptic plasticity as the average of synaptic changes across TBS-activated synapses. We used the aforementioned calculations to calculate synaptic plasticity in M1 and M2.

We then modeled resource depletion due to network activity and its resulting homeostatic effect on plasticity following [35]. This model, which we refer to as model 3 (M3), assumes that plasticity at individual synapses depends on a resource that is shared by the whole network and is depleted by elevated network

Table 2
Parameters for voltage-based plasticity rule.

Parameter	Value	Explanation
A_{LTD}	0.36 mV^{-1}	LTD rate
A_{LTP}	0.16 mV^{-2}	LTP rate
θ_-	−62 mV	LTD threshold
θ_+	−44 mV	LTP threshold
τ_x	6 ms	presynaptic input trace lowpass time constant
τ_-	12 ms	LTD voltage trace lowpass time constant
τ_+	5 ms	LTP voltage trace lowpass time constant
k	20 Hz	depletion rate constant
τ_α	2.5 ms	Filter time constant for the network spiking
τ_η	100 ms	Recovery time constant of resource availability
η^*	0.57	LTP-LTD reversal point
m	0.03	Steepness of reversal

activity. The equilibrated resource availability η_0 is obtained for a given fixed average network firing rate α by:

$$\eta_0(\alpha) = \left(1+\frac{\alpha}{k}\right)^{-1}$$

where k is the depletion rate constant. The dynamics of the shared resource availability $\eta(t)$ were modeled as:

$$\frac{d\eta(t)}{dt} = \frac{\eta_0(\alpha(t)) - \eta(t)}{\eta_0(\alpha(t))\cdot\tau_\eta}$$

in which $\alpha(t)$ is network firing after it has been low-pass filtered and normalized by $N_{network}$, the number of synapses activated by network activity as:

$$\tau_\alpha\frac{\alpha(t)}{dt} = -\alpha(t) + \frac{\delta\left(t-t_{spike}\right)}{N_{network}}$$

where $\delta(t-t_{spike})$ is equal to one when a synapse is activated and τ_α represents the filter time constant for the network activity. In addition, $\eta_0(\alpha(t))$ is the steady-state resource availability for average network spiking $\alpha(t)$. To augment the plasticity rule, we scaled synaptic weight changes Δw_i by $\gamma(\eta(t))$

$$\Delta w_i = \gamma(\eta(t))\cdot\Delta w_i$$

where $\gamma(\eta(t))$ is a sigmoidal resource modulation function as:

$$\gamma(\eta(t)) = \frac{2}{1+exp\left(\frac{\eta^*-\eta(t)}{m}\right)} - 1$$

Where η^* sets the LTP-LTD reversal point and m is the steepness of the reversal.

Normalized synaptic efficacy

To induce synaptic changes in the CA1 pyramidal neuron we model a synaptic input to the Schaffer collateral synapses (selected at random) with a TBS pulse train. TBS consisted of bursts of 5 pulses at 100 Hz, with each burst repeated 5 times at 5 Hz. This pulse train (epoch) was applied 3 times in our experiments with intervals of 30 s, while in the model only a single TBS epoch was applied to reduce computation times. Synaptic efficacy before and after the TBS are averaged across synapses and divided to give the normalized synaptic efficacy (change) analogous to the normalized EPSP in the experiment.

Credit author statement

Forouzan Farahani: Methodology, Conducting Experiment, Computational Modeling, Formal analysis, Investigation, Writing - Original Draft, Visualization.

Greg Kronberg: Methodology, Computational Modeling, Resources, Writing - Review & Editing.

Mohamad FallahRad: Methodology, Resources, Review & Editing.

Hysell Oveido: Methodology, Resources, Writing - Review & Editing.

Lucas C Parra: Conceptualization, Methodology, Supervision, Writing - Review & Editing.

Declaration of competing interest

We wish to confirm that there are no known conflicts of interest associated with this publication and there has been no significant financial support for this work that could have influenced its outcome.

Acknowledgments

This work was supported by the NIH through grant # R01NS095123. We would like to thank Marom Bikson for his invaluable help in brainstorming ideas specifically injecting current as an intervention in our experiment.

References

[1] Nitsche MA, Cohen LG, Wassermann EM, Priori A, Lang N, Antal A, et al. Transcranial direct current stimulation: state of the art 2008. Brain Stimul 2008;1:206–23. https://doi.org/10.1016/j.brs.2008.06.004.
[2] Santarnecchi E, Brem A-K, Levenbaum E, Thompson T, Kadosh RC, Pascual-Leone A. Enhancing cognition using transcranial electrical stimulation. Curr Opin Behav Sci 2015;4:171–8. https://doi.org/10.1016/j.cobeha.2015.06.003.
[3] Lefaucheur J-P, Antal A, Ayache SS, Benninger DH, Brunelin J, Cogiamanian F, et al. Evidence-based guidelines on the therapeutic use of transcranial direct current stimulation (tDCS). Clin Neurophysiol Off J Int Fed Clin Neurophysiol 2017;128:56–92. https://doi.org/10.1016/j.clinph.2016.10.087.
[4] Lucena MFG, Teixeira PEP, Bonin Pinto C, Fregni F. Top 100 cited noninvasive neuromodulation clinical trials. Expet Rev Med Dev 2019;16:451–66. https://doi.org/10.1080/17434440.2019.1615440.
[5] Bucur M, Papagno C. Are transcranial brain stimulation effects long-lasting in post-stroke aphasia? A comparative systematic review and meta-analysis on naming performance. Neurosci Biobehav Rev 2019;102:264–89. https://doi.org/10.1016/j.neubiorev.2019.04.019.
[6] Jackson MP, Rahman A, Lafon B, Kronberg G, Ling D, Parra LC, et al. Animal models of transcranial direct current stimulation: Methods and mechanisms. Clin Neurophysiol 2016;127:3425–54. https://doi.org/10.1016/j.clinph.2016.08.016.
[7] Liu A, Vöröslakos M, Kronberg G, Henin S, Krause MR, Huang Y, et al. Immediate neurophysiological effects of transcranial electrical stimulation. Nat Commun 2018;9:5092. https://doi.org/10.1038/s41467-018-07233-7.
[8] Huang Y, Liu AA, Lafon B, Friedman D, Dayan M, Wang X, et al. Measurements and models of electric fields in the in vivo human brain during transcranial electric stimulation. ELife 2017;6:e18834. https://doi.org/10.7554/eLife.18834.
[9] Jackson MP, Rahman A, Lafon B, Kronberg G, Ling D, Parra LC, et al. Animal models of transcranial direct current stimulation: Methods and mechanisms. Clin Neurophysiol 2016;127:3425–54. https://doi.org/10.1016/j.clinph.2016.08.016.
[10] Sun Y, Lipton JO, Boyle LM, Madsen JR, Goldenberg MC, Pascual-Leone A, et al. Direct current stimulation induces mGluR5-dependent neocortical plasticity: cathodal DCS Induces LTD. Ann Neurol 2016;80:233–46. https://doi.org/10.1002/ana.24708.
[11] Kronberg G, Bridi M, Abel T, Bikson M, Parra LC. Direct current stimulation modulates LTP and LTD: activity dependence and dendritic effects. Brain Stimul 2017;10:51–8. https://doi.org/10.1016/j.brs.2016.10.001.
[12] Kronberg G, Rahman A, Sharma M, Bikson M, Parra LC. Direct current stimulation boosts hebbian plasticity in vitro. Brain Stimul 2020;13:287–301. https://doi.org/10.1016/j.brs.2019.10.014.
[13] Agboada D, Mosayebi Samani M, Jamil A, Kuo M-F, Nitsche MA. Expanding the parameter space of anodal transcranial direct current stimulation of the primary motor cortex. Sci Rep 2019;9:18185. https://doi.org/10.1038/s41598-019-54621-0.

[14] Mosayebi Samani M, Agboada D, Jamil A, Kuo M-F, Nitsche MA. Titrating the neuroplastic effects of cathodal transcranial direct current stimulation (tDCS) over the primary motor cortex. Cortex 2019;119:350–61. https://doi.org/10.1016/j.cortex.2019.04.016.
[15] Stagg CJ, Nitsche MA. Physiological basis of transcranial direct current stimulation. Neuroscientist 2011;17:37–53. https://doi.org/10.1177/1073858410386614.
[16] Fritsch B, Reis J, Martinowich K, Schambra HM, Ji Y, Cohen LG, et al. Direct current stimulation promotes BDNF-dependent synaptic plasticity: potential implications for motor learning. Neuron 2010;66:198–204. https://doi.org/10.1016/j.neuron.2010.03.035.
[17] Marquez-Ruiz J, Leal-Campanario R, Sanchez-Campusano R, Molaee-Ardekani B, Wendling F, Miranda PC, et al. Transcranial direct-current stimulation modulates synaptic mechanisms involved in associative learning in behaving rabbits. Proc Natl Acad Sci Unit States Am 2012;109:6710–5. https://doi.org/10.1073/pnas.1121147109.
[18] Buzsáki G, Moser EI. Memory, navigation and theta rhythm in the hippocampal-entorhinal system. Nat Neurosci 2013;16:130–8. https://doi.org/10.1038/nn.3304.
[19] Litwin-Kumar A, Doiron B. Formation and maintenance of neuronal assemblies through synaptic plasticity. Nat Commun 2014;5:5319. https://doi.org/10.1038/ncomms6319.
[20] Holtmaat A, Caroni P. Functional and structural underpinnings of neuronal assembly formation in learning. Nat Neurosci 2016;19:1553–62. https://doi.org/10.1038/nn.4418.
[21] Malenka RC, Bear MF. LTP and LTD. Neuron 2004;44:5–21. https://doi.org/10.1016/j.neuron.2004.09.012.
[22] Ziemann U. Learning modifies subsequent induction of long-term potentiation-like and long-term depression-like plasticity in human motor cortex. J Neurosci 2004;24:1666–72. https://doi.org/10.1523/JNEUROSCI.5016-03.2004.
[23] Terzuolo CA, Bullock TH. Measurement OF imposed voltage gradient adequate to modulate neuronal firing. Proc Natl Acad Sci Unit States Am 1956;42:687–94. https://doi.org/10.1073/pnas.42.9.687.
[24] Reato D, Rahman A, Bikson M, Parra LC. Low-intensity electrical stimulation affects network dynamics by modulating population rate and spike timing. J Neurosci 2010;30:15067–79. https://doi.org/10.1523/JNEUROSCI.2059-10.2010.
[25] Vöröslakos M, Takeuchi Y, Brinyiczki K, Zombori T, Oliva A, Fernández-Ruiz A, et al. Direct effects of transcranial electric stimulation on brain circuits in rats and humans. Nat Commun 2018;9:483. https://doi.org/10.1038/s41467-018-02928-3.
[26] Kim Y, Hsu C-L, Cembrowski MS, Mensh BD, Spruston N. Dendritic sodium spikes are required for long-term potentiation at distal synapses on hippocampal pyramidal neurons. ELife 2015;4:e06414. https://doi.org/10.7554/eLife.06414.
[27] Bikson M, Inoue M, Akiyama H, Deans JK, Fox JE, Miyakawa H, et al. Effects of uniform extracellular DC electric fields on excitability in rat hippocampal slices in vitro: modulation of neuronal function by electric fields. J Physiol 2004;557:175–90. https://doi.org/10.1113/jphysiol.2003.055772.
[28] Golding NL, Staff NP, Spruston N. Dendritic spikes as a mechanism for cooperative long-term potentiation. Nature 2002;418:326–31. https://doi.org/10.1038/nature00854.
[29] Radman T, Ramos RL, Brumberg JC, Bikson M. Role of cortical cell type and morphology in subthreshold and suprathreshold uniform electric field stimulation in vitro. Brain Stimul 2009;2:215–28. https://doi.org/10.1016/j.brs.2009.03.007. e3.
[30] Berzhanskaya J, Chernyy N, Gluckman BJ, Schiff SJ, Ascoli GA. Modulation of hippocampal rhythms by subthreshold electric fields and network topology. J Comput Neurosci 2013;34:369–89. https://doi.org/10.1007/s10827-012-0426-4.
[31] Kirkwood A, Dudek SM, Gold JT, Aizenman CD, Bear MF. Common forms of synaptic plasticity in the hippocampus and neocortex in vitro. Science 1993;260:1518–21. https://doi.org/10.1126/science.8502997.
[32] Sjöström PJ, Turrigiano GG, Nelson SB. Rate, timing, and cooperativity jointly determine cortical synaptic plasticity. Neuron 2001;32:1149–64. https://doi.org/10.1016/s0896-6273(01)00542-6.
[33] Takahashi H, Magee JC. Pathway interactions and synaptic plasticity in the dendritic tuft regions of CA1 pyramidal neurons. Neuron 2009;62:102–11. https://doi.org/10.1016/j.neuron.2009.03.007.
[34] Clopath C, Büsing L, Vasilaki E, Gerstner W. Connectivity reflects coding: a model of voltage-based STDP with homeostasis. Nat Neurosci 2010;13:344–52. https://doi.org/10.1038/nn.2479.
[35] Delattre V, Keller D, Perich M, Markram H, Muller EB. Network-timing-dependent plasticity. Front Cell Neurosci 2015;9. https://doi.org/10.3389/fncel.2015.00220.
[36] Nitsche MA, Müller-Dahlhaus F, Paulus W, Ziemann U. The pharmacology of neuroplasticity induced by non-invasive brain stimulation: building models for the clinical use of CNS active drugs. J Physiol 2012;590:4641–62. https://doi.org/10.1113/jphysiol.2012.232975.
[37] Megías M, Emri Z, Freund TF, Gulyás AI. Total number and distribution of inhibitory and excitatory synapses on hippocampal CA1 pyramidal cells. Neuroscience 2001;102:527–40. https://doi.org/10.1016/s0306-4522(00)00496-6.
[38] Amaral DG, Witter MP. The three-dimensional organization of the hippocampal formation: a review of anatomical data. Neuroscience 1989;31:571–91. https://doi.org/10.1016/0306-4522(89)90424-7.
[39] Knowles W, Schwartzkroin P. Axonal ramifications of hippocampal Ca1 pyramidal cells. J Neurosci 1981;1:1236–41. https://doi.org/10.1523/JNEUROSCI.01-11-01236.1981.
[40] Cakan C, Obermayer K. Biophysically grounded mean-field models of neural populations under electrical stimulation. PLoS Comput Biol 2020;16:e1007822. https://doi.org/10.1371/journal.pcbi.1007822.
[41] Brunel N. Dynamics of sparsely connected networks of excitatory and inhibitory spiking neurons. J Comput Neurosci 2000;8:183–208. https://doi.org/10.1023/a:1008925309027.
[42] Rubin DB, Van Hooser SD, Miller KD. The stabilized supralinear network: a unifying circuit motif underlying multi-input integration in sensory cortex. Neuron 2015;85:402–17. https://doi.org/10.1016/j.neuron.2014.12.026.
[43] Renart A, de la Rocha J, Bartho P, Hollender L, Parga N, Reyes A, et al. The asynchronous state in cortical circuits. Science 2010;327:587–90. https://doi.org/10.1126/science.1179850.
[44] Reato D, Bikson M, Parra LC. Lasting modulation of in vitro oscillatory activity with weak direct current stimulation. J Neurophysiol 2015;113:1334–41. https://doi.org/10.1152/jn.00208.2014.
[45] Keck T, Toyoizumi T, Chen L, Doiron B, Feldman DE, Fox K, et al. Integrating Hebbian and homeostatic plasticity: the current state of the field and future research directions. Philos Trans R Soc B Biol Sci 2017;372:20160158. https://doi.org/10.1098/rstb.2016.0158.
[46] Lu H, Gallinaro JV, Rotter S. Network remodeling induced by transcranial brain stimulation: a computational model of tDCS-triggered cell assembly formation. Netw Neurosci Camb Mass 2019;3:924–43. https://doi.org/10.1162/netn_a_00097.
[47] Rahman A, Lafon B, Parra LC, Bikson M. Direct current stimulation boosts synaptic gain and cooperativity in vitro: DCS boosts synaptic gain and cooperativity. J Physiol 2017;595:3535–47. https://doi.org/10.1113/JP273005.
[48] Nitsche MA, Jaussi W, Liebetanz D, Lang N, Tergau F, Paulus W. Consolidation of human motor cortical neuroplasticity by D-cycloserine. Neuropsychopharmacology 2004;29:1573–8. https://doi.org/10.1038/sj.npp.1300517.
[49] Boroda E, Sponheim SR, Fiecas M, Lim KO. Transcranial direct current stimulation (tDCS) elicits stimulus-specific enhancement of cortical plasticity. Neuroimage 2020;211:116598. https://doi.org/10.1016/j.neuroimage.2020.116598.
[50] Kang N, Summers JJ, Cauraugh JH. Transcranial direct current stimulation facilitates motor learning post-stroke: a systematic review and meta-analysis. J Neurol Neurosurg Psychiatry 2016;87:345–55. https://doi.org/10.1136/jnnp-2015-311242.
[51] Raymond CR, Redman SJ. Spatial segregation of neuronal calcium signals encodes different forms of LTP in rat hippocampus. J Physiol 2006;570:97–111. https://doi.org/10.1113/jphysiol.2005.098947.
[52] Hines ML, Carnevale NT. The NEURON simulation environment. Neural Comput 1997;9:1179–209. https://doi.org/10.1162/neco.1997.9.6.1179.
[53] Apostolides PF, Milstein AD, Grienberger C, Bittner KC, Magee JC. Axonal filtering allows reliable output during dendritic plateau-driven complex spiking in CA1 neurons. Neuron 2016;89:770–83. https://doi.org/10.1016/j.neuron.2015.12.040.